Significant role of spin-triplet state for exciton dissociation in organic solids

Yamanaka, Takahiko
Central Research Laboratory, Hamamatsu Photonics K.K.

Nakanotani, Hajime
Center for Organic Photonics and Electronics Research, Kyushu University

Adachi, Chihaya
Center for Organic Photonics and Electronics Research, Kyushu University

出版情報：Science Advances. 8 (9), 2022-03-04. American Association for the Advancement of Science (AAAS)
バージョン：

MATERIALS SCIENCE

Significant role of spin-triplet state for exciton dissociation in organic solids

Takahiko Yamanaka[1,2], Hajime Nakanotani[2,3]*, Chihaya Adachi[2,3]*

Clarification of the role of the spin state that initiates exciton dissociation is critical to attaining a fundamental understanding of the mechanism of organic photovoltaics. Although an excited spin-triplet state with an energy lower than that of excited spin-singlet state is disadvantageous in exciton dissociation, a small electron exchange integral results in small singlet-triplet energy splitting in some material systems. This energy splitting leads to a nearly isoenergetic alignment of both excited states, raising a question about the role of excited spin states in exciton dissociation. Herein, we show that the spin-triplet rather than the spin-singlet plays a critical role in the exciton dissociation that leads to the formation of free carriers. This result indicates that the spin-triplet inherently acts as an intermediate, leading to exciton dissociation. Thus, our demonstration provides a fundamental understanding of the role of excited spin states of organic molecular systems in photoinduced charge-carrier generation.

INTRODUCTION

The role of spin states in the excited states of organic semiconductor materials has been extensively studied to elucidate the unique exciton dynamics inherent to the tightly bonded hole-electron pair in organic molecular systems. In particular, in organic optoelectronic devices such as organic light-emitting diodes (OLEDs) and organic photovoltaics (OPVs), manipulating the excited spin states is critical for improving device performance (*1*–*4*). For example, the formation of low-energy triplet excitons via recombination of a photogenerated hole-electron pair is generally considered a major energy-loss pathway in donor-acceptor (D-A) blend-type bulk heterojunction OPVs (BHJ-OPVs) (Fig. 1A), leading to a low carrier extraction yield (*3*–*7*). Thus, the rapid dissociation of excitons and the successive suppression of bimolecular recombination of the separated charge carriers have been widely considered to be requisites for OPVs with high photocarrier generation efficiency. Some state-of-the-art BHJ-OPVs have demonstrated nearly unity internal quantum efficiency (IQE) for photocarrier generation (*8*–*10*). However, in primarily charge-transfer (CT)–type excited spin states, it remains controversial which excited spin states play a critical role in exciton dissociation; various aspects of the role of excited spin states have therefore been investigated to attain a comprehensive understanding (*11*–*13*).

In general, an excited spin-triplet state with an energy lower than that of an excited spin-singlet state is disadvantageous for exciton dissociation events because it requires an input of external energy greater than the exciton binding energy of the excited spin-triplet state (*14*). By contrast, the excited-state lifetime of an excited spin-triplet state is much longer than that of an excited spin-singlet state because of the weak spin-orbit coupling in molecules. Because exciton dissociation by an external electric field occurs within the exciton lifetime of molecules, their exciton lifetime should influence the exciton dissociation process (*15*). Therefore, if the energy level of an excited spin-triplet is nearly isoenergetically aligned with that of an excited spin-singlet, the question arises as to which excited spin state is advantageous for the charge separation events following the formation of the exciton (Fig. 1A). This question has not yet been clarified for organic solid-state films, even though answering this question is critical for completely suppressing exciton losses in OPVs.

The ideal energy alignment of excited spin states in organic molecules and solid composites can be realized by a small electron exchange integral in their excited states. A proper combination of electron-donating (D) and electron-accepting (A) units in molecular systems can well control the energy splitting between the lowest excited spin-singlet (S_1) state and the lowest excited spin-triplet (T_1) state (ΔE_{ST}), resulting in a ΔE_{ST} of tens of milli–electron volts. In these molecular systems, since the S_1 and T_1 states generally have a lowest CT excited-state character ($^1CT_1$ and $^3CT_1$) and the energy is sufficiently lower than that of the locally excited spin-triplet state of a D or an A unit ($^3LE_1$), intramolecular CT states are formed for both spin states when the molecule is excited optically or electrically. Then, the CT exciton can dissociate and diffuse to the adjacent molecules as a free carrier if the CT exciton overcomes the Coulomb binding energy, depicting the footprints of charge separation behavior. Therefore, such systems should provide an ideal platform to explore the role of excited spin states for understanding exciton dissociation processes.

A series of excitonic processes from exciton generation to charge separation (exciton dissociation) and recombination events similar to those in OPVs can be observed in organic thin films even without the aid of an external electrical field if the solid film is made of a molecular system that exhibits spontaneous orientation polarization (SOP) (Fig. 1B) (*16*). The SOP induced by a spontaneous ordering of a permanent dipole moment of the molecules forms an internal potential slope of the electrical field (*17*), working as a driving force in the charge separation. In this case, the recombination of photogenerated holes and electrons can be detected as long-lived luminescence, which can be categorized as previously reported long persistent luminescence (LPL) (*18*). Although the fundamental driving force for LPL is attributed to charge separation based mainly on the Coulomb interaction between donor and acceptor molecules, the aforementioned long-lived emission (LLE) relies not only on the intermolecular Coulomb interaction but also substantially on the electric field that arises from SOP. In our previous work, the LLE

[1]Central Research Laboratory, Hamamatsu Photonics K.K., 5000 Hirakuchi, Hamakita-ku, Hamamatsu, Shizuoka 434-8601, Japan. [2]Center for Organic Photonics and Electronics Research (OPERA), Kyushu University, 744 Motooka, Nishi-ku, Fukuoka 819-0395, Japan. [3]International Institute for Carbon Neutral Energy Research (WPI-I[2]CNER), Kyushu University, 744 Motooka, Nishi-ku, Fukuoka 819-0395, Japan.
*Corresponding author. Email: nakanotani@cstf.kyushu-u.ac.jp (H.N.); adachi@cstf.kyushu-u.ac.jp (C.A.)

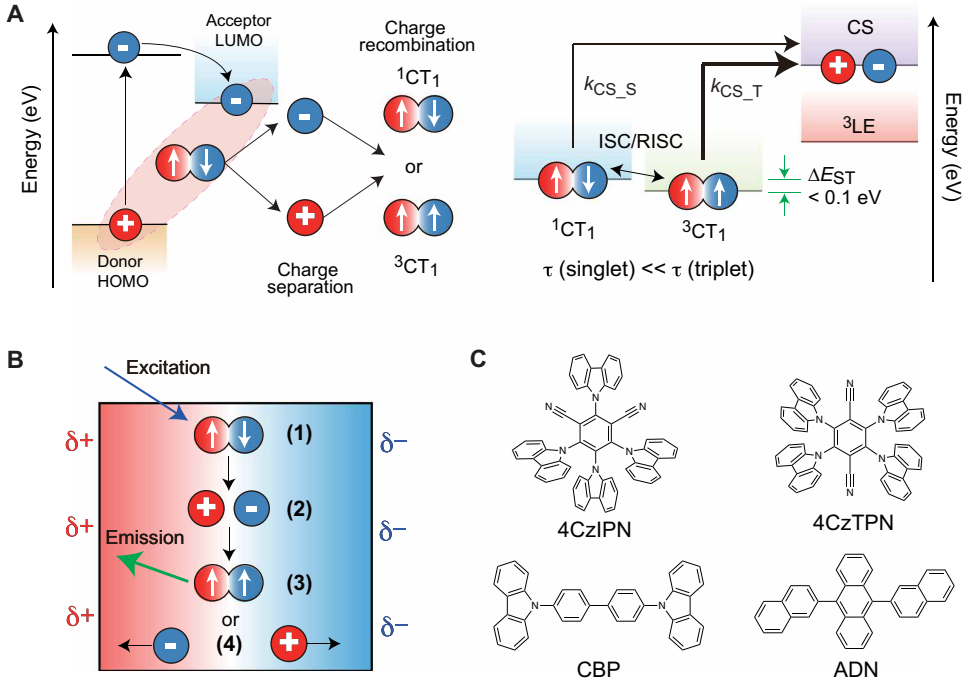

Fig. 1. Key photophysical process of charge-transfer–type exciton. (**A**) Left: Photophysical process in an organic D-A system, i.e., photocarrier generation via dissociation of the charge-transfer exciton (CTE) and the formation of $^1CT_1$ and $^3CT_1$ via bimolecular recombination during carrier diffusion. Right: Excited-state energy-level diagram to investigate the role of the excited spin state in the exciton dissociation process. Here, CS and τ represent the carrier separation state and the exciton lifetime, respectively. ISC, intersystem crossing; RISC, reverse intersystem crossing; HOMO, highest occupied molecular orbital; LUMO, lowest unoccupied molecular orbital. (**B**) Schematic of spontaneous exciton dissociation in a polar organic film. Process (1): CTE generation by photoexcitation. Process (2): Spontaneous dissociation of the CTE by the SOP of the film. Process (3): Bimolecular recombination between the dissociated carriers. Process (4): Charge-carrier diffusion and accumulation at the interface. (**C**) Molecular structures of the compounds used in this study. 4CzIPN, 2,4,5,6-tetra(9H-carbazol-9-yl)iso-phthalonitrile; 4CzTPN, 1,2,4,5-tetrakis(carbazol-9-yl)-3,6-dicyanobenzene; ADN, 9,10-bis(2-naphthyl)anthracene; CBP, 4,4′-bis(*N*-carbazolyl)-1,1′-biphenyl.

reveals the presence of a nonnegligible photoluminescence (PL) quenching process in a solid-state film containing a polar fluorophore composed of a D-A combination. However, a deeper understanding regarding the role of the spin state for the exciton dissociation process had been unreachable. Hence, in the present study, conventional time-resolved PL (TRPL) measurements are conducted to elucidate the role of excited spin states on spontaneous exciton dissociation in polar organic films that exhibit SOP and a small ΔE_{ST}. Our work clarifies that excited spin-triplet states act as an efficient "intermediate excited-state bath," leading to the successive exciton dissociation process in solid thin films.

RESULTS

Figure 1C and fig. S2 show the chemical structures and the energy levels for two fluorophores and two wide-energy-gap molecules used as emitters and host matrices, respectively. Because 2,4,5,6-tetra(9H-carbazol-9-yl)iso-phthalonitrile (4CzIPN) and 1,2,4,5-tetrakis(carbazol-9-yl)-3,6-dicyanobenzene (4CzTPN) have a small ΔE_{ST} of 0.01 and 0.06 eV, respectively, these molecules are well known to function as efficient thermally activated delayed fluorescence (TADF) emitters in OLEDs (*2*, *19*). Note that 4CzIPN has a permanent dipole moment (μ_D = 3.8 Debye), whereas 4CzTPN is a nonpolar molecule because of its symmetric molecular structure. For the host matrix, 4,4′-bis(*N*-carbazolyl)-1,1′-biphenyl (CBP) was chosen as a triplet-activated host because the T_1 state of CBP (2.55 eV) is higher than those of 4CzIPN (2.48 eV) and 4CzTPN (2.28 eV). By contrast, because the T_1 state for 9,10-bis(2-naphthyl)anthracene (ADN) (1.69 eV) (*20*) is much lower than those for 4CzIPN and 4CzTPN but the S_1 state can confine the S_1 states for 4CzIPN and 4CzTPN, the ADN matrix functions as a triplet-scavenging host (fig. S2).

Figure 2A shows the TRPL profiles for 4CzIPN or 4CzTPN doped into a CBP host matrix with a doping concentration of 50 weight % (wt %). Here, the excitation light with a wavelength of 430 nm was used to directly excite the absorption band of the fluorophores (fig. S3). In the case of the 4CzIPN:CBP film, after the photoexcitation light was turned off, two components in the emission decay were observed in the measurement time range of ~2 ms: an inherent radiative decay due to 4CzIPN (i.e., delayed fluorescence of singlet excitons generated via a reverse intersystem crossing from the T_1 state) and an LLE decay arising from slow recombination of charge carriers dissociated from the 4CzIPN excitons (see schematic in Fig. 1B). Note that the prompt decay component based on the singlet excitons in 4CzIPN is buried in the first component because of the nanosecond decay. By contrast, no LLE was observed in the profile of the 4CzTPN:CBP film. Here, we conducted atomic force microscopy measurements to confirm the microstructures of each film (fig. S4). The almost flat surface with the average roughness between 0.28 and 0.36 nm was observed in all films, indicating no substantial difference in the microstructures.

First, the absence of LLE in the 4CzTPN:CBP film is attributed to the lack of an SOP, i.e., interfacial charge density (σ_{int}), in the film.

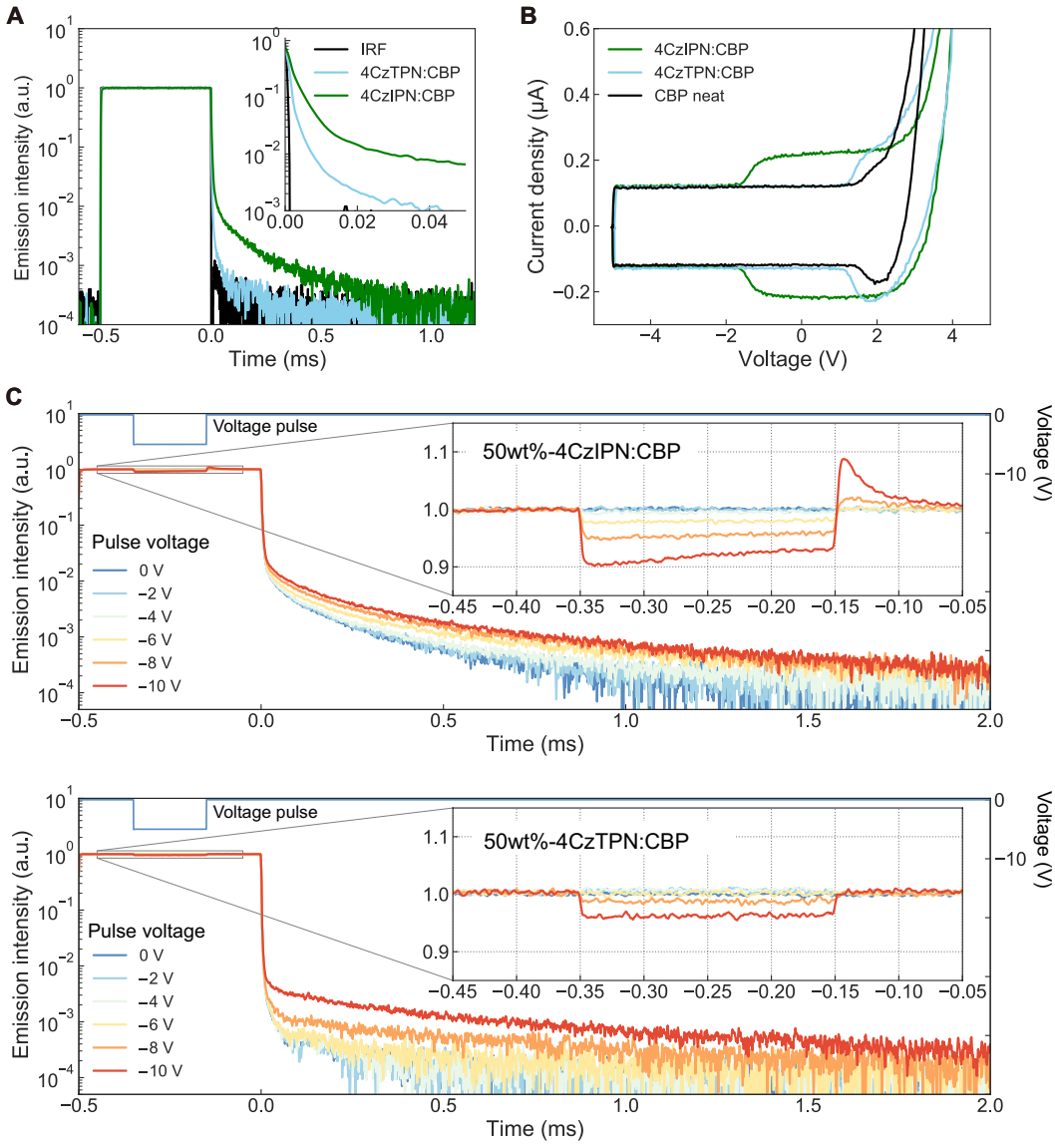

Fig. 2. Photoluminescence characteristics of 4CzIPN and 4CzTPN in a triplet-activated CBP host matrix. (**A**) TRPL profiles of 4CzIPN:CBP and 4CzTPN:CBP blend films. A 430-nm LED was used as excitation light, and the light pulse width and the power were fixed at 500 μs and 20 mW cm^{-2}, respectively. The lifetime of the LLE component is much longer than the intrinsic TADF lifetime for 4CzIPN. IRF, instrument response function. (**B**) Displacement current measurement profiles of the 4CzIPN- and 4CzTPN-based diodes. The doping concentration of each fluorophore was fixed at 50 wt %. (**C**) Electrically modulated TRPL profile in noncarrier-injecting (NCI)–type devices based on CBP:4CzIPN (top) and CBP:4CzTPN (bottom). A negative voltage pulse with different voltages with a pulse width of 200 μs was applied to the sample during photoexcitation. The inset shows an enlarged view of the TRPL profile during photoexcitation. a.u., arbitrary units.

To calculate the σ_{int}, displacement current measurements (DCMs) (*21*) were conducted for a diode with a configuration of indium tin oxide (ITO) (100 nm)/4,4′-bis(*N*-(1-naphthyl)-*N*-phenylamino)-biphenyl (α-NPD) (50 nm)/4CzIPN:CBP or 4CzTPN:CBP (50 nm)/Al (100 nm). The onset voltage was lower than 0 V for the 4CzIPN:CBP diode, as shown in Fig. 2B, which is attributed to charge accumulation ($\sigma_{int} = -1.79$ mC m^{-2}) at the α-NPD/CBP:4CzIPN interface (*17*), indicating the occurrence of SOP inside the 4CzIPN:CBP layer. Because no net carrier accumulation at the α-NPD/CBP:4CzTPN interface was observed from the current density–voltage characteristics (Fig. 2B), these results indicate that the occurrence of SOP in the film is a critical mechanism for the spontaneous dissociation of the excitons.

Notably, the excitons of both fluorophores can also dissociate upon application of an external voltage to the films, which is similar to the case of OPVs. Figure 2C shows the TRPL profiles recorded when a negative voltage pulse (200-μs width) was applied during photoexcitation in noncarrier-injecting (NCI)–type devices with a structure of ITO (100 nm)/2,4,6-tris(biphenyl-3-yl)-1,3,5-triazine (T2T) (30 nm)/4CzIPN:CBP or 4CzTPN:CBP (100 nm)/CBP (30 nm)/Al (100 nm) (fig. S2C). For both fluorophores, the steady-state PL intensity during photoexcitation was attenuated by the external voltage pulse, clearly indicating the occurrence of exciton dissociation (inset of Fig. 2C). After the excitation light was turned off, the LLE was observed even in the 4CzTPN:CBP NCI device with an

applied external negative voltage during photoexcitation. The LLE appearance was attributed to the photogeneration of excitons and subsequent exciton dissociation into holes and electrons because of the external bias. An electric field–modulated electroluminescence (EL) enhancement was also observed for the 4CzTPN:CBP NCI device under a negative voltage offset, whereas no EL spike was observed at 0 V offset (fig. S5). Therefore, these observations indicate that the charge carriers generated by the dissociation of excitons can essentially maintain a stable state at least on the millisecond time scale in both triplet-activated films.

Next, we discuss the role of the excited spin states on the exciton dissociation process. We first investigate the role of the $^3CT_1$ of 4CzIPN on the dissociation process by incorporating ADN as a triplet-scavenging host molecule. Notably, the σ_{int} of a 4CzIPN:ADN layer (-1.56 mC m^{-2}) is similar to that of a 4CzIPN:CBP layer (-1.79 mC m^{-2}), indicating the same level of SOP for both films (fig. S6A). The TADF component of 50-wt%-4CzIPN doped in the ADN host is substantially quenched (fig. S7), resulting in a PL quantum yield (PLQY) of 15% that corresponds to the prompt (fluorescence) PLQY in the 4CzIPN:CBP film (28%). This result indicates that the triplet excitons of 4CzIPN are substantially quenched by the $^3LE_1$ of ADN via Dexter-type triplet energy transfer (*22*).

The LLE component was substantially diminished in the TRPL profile for the 4CzIPN:ADN film (Fig. 3A), indicating that the unique photophysical characteristics of ADN control the disappearance of the photogenerated holes and electrons in the 4CzIPN:ADN film. We can attribute this phenomenon to either (i) the low exciton dissociation yield in the triplet-deactivated film or (ii) the nonradiative decay from the $^3LE_1$ of ADN. The arguments for these hypotheses are discussed as follows:

1) The SOP for a 4CzIPN:CBP film becomes larger nonlinearly with increasing concentration of polar 4CzIPN molecules (fig. S6B) because of the peculiar intermolecular dipole–dipole interaction between neighboring 4CzIPN molecules (*23*, *24*), whereas the LLE decay in TRPL becomes shorter (fig. S8). The attenuation of the LLE component with increasing 4CzIPN concentration implies that fewer charge carriers are dissociated from the 4CzIPN excitons. However, the LLE intensity should be influenced not only by the charge-carrier density but also by the change in carrier recombination probability, which depends on the trap density or carrier transport ability of the film. Hence, to study the charge separation dynamics in greater detail, we conducted PLQY measurements of 4CzIPN:CBP films (Fig. 3B). The PLQY for the TADF component (i.e., the contribution of $^3CT_1$) decreases with increasing doping concentration, whereas the PLQY for the prompt component remains almost the same, suggesting that the number of active triplet excitons is correlated with the dissociation probability. We then evaluated the electrical field–modulated TRPL in the 50-wt%-4CzIPN:CBP and the neat 4CzIPN NCI devices to directly confirm the spin-selective exciton dissociation. Even though the steady-state PL intensity for the 50-wt%-4CzIPN:CBP NCI device was lowered when an external voltage pulse was applied, as illustrated in the inset of Fig. 2C, the neat 4CzIPN NCI device was unaffected by applying an external electric field (fig. S9). Furthermore, the delayed component (intrinsic delayed fluorescence lifetime via $^3CT_1$) in the 50-wt%-4CzIPN:CBP NCI device with a negative voltage was appreciably attenuated compared with that of the device without an electric field, whereas the prompt decay component was unchanged (Fig. 3C). Also, virtually no electrical field modulation of either the prompt or the delayed component was observed in the TRPL profiles of the 4CzIPN neat NCI device (Fig. 3D). Notably, in the case of the neat films, although the SOP is larger than the doped films as indicated by fig. S6B, some of the 4CzIPN molecules should have been insusceptible to SOP and external electric fields due to the cancellation of the dipoles or no specific interaction with CBP molecules. These results clearly suggest that the charge separation event after the formation of the excitonic states occurs selectively via the excited spin-triplet state and that the dissociation probability of the singlet excitons, contributing to the rapid radiative relaxation, is negligibly low (Fig. 3E). The relaxation time of the PL quenching after applying the external electric field is over several microseconds in the 4CzIPN:CBP NCI device, indicating that the charge carriers are formed slowly (fig. S10).

Because the $^3CT_1$ lifetime (τ_d) of 2.3 μs is appreciably longer than the $^1CT_1$ lifetime (τ_p) of 30 ns in the case of 50-wt%-4CzIPN:CBP, we interpret this phenomenon as the spontaneous exciton dissociation from the long-lived $^3CT_1$ of 4CzIPN, which would be favorable compared with dissociation from the energetically closed $^1CT_1$. Notably, the radiative decay from the $^1CT_1$ to the ground state with a rate constant (k_r) of 9.3×10^6 (s^{-1}) and the intersystem crossing with a rate constant (k_{ISC}) of 2.4×10^7 (s^{-1}) should both be faster than the exciton dissociation in this molecular system. However, we considered that the low dissociation probability in the 4CzIPN neat is attributable to the competition between the exciton dissociation and the nonradiative relaxation in the triplet excited state. Several groups have reported that concentration quenching of 4CzIPN is due to intermolecular interaction that originates from an electron exchange between neighboring molecules following a nonradiative decay from the T_1 to the ground state (*25*, *26*). According to the literature (*25*), the molecular distances of 50-wt%-4CzIPN:CBP and neat 4CzIPN can be calculated to be 1.4 and 1.0 nm, respectively. Then, we estimated the rate constant of Dexter energy transfer (k_{DET}) by assuming the effective exciton radius of ~1 nm. The k_{DET} of a 4CzIPN neat film was calculated to be 2.2 times higher than that of a 50-wt%-4CzIPN doped film at least, implying that the concentration quenching is accelerated sufficiently (refer to Supplementary Information). Although the dependence of PLQY on the 4CzIPN doping concentration (Fig. 3B) shares a similar trend with the result in the literature (*25*), note that the absolute value of PLQY in the literature (*25*) is much lower than that of our results especially in the high-doping concentration region. One possibility for the origin of the difference of PLQY is speculated to be a difference in material purity because the PL characteristics of organic material are extremely sensitive to its purity. Although it is impossible to directly compare the material purity, we note that all experiments in this study were carried out using the highly purified 4CzIPN powder with the guaranteed traceability for the purity (fig. S11). In addition, to obtain supplementary evidence for the dissociation from triplet excited states, we studied a 50-wt%-tris-(8-hydroxyquinoline)aluminum (Alq_3):CBP NCI device that completely deactivates triplet excitons. Because the steady-state PL intensity in this device was unchanged when an external electric field was applied, as in the case of the 4CzIPN neat NCI device (fig. S12), the low dissociation probability for singlet excitons is again confirmed.

We also observed the electric field–modulated EL enhancement in the 4CzIPN NCI devices (fig. S13). The EL spike intensity for the 50-wt%-4CzIPN:CBP NCI device was greater than that for the neat

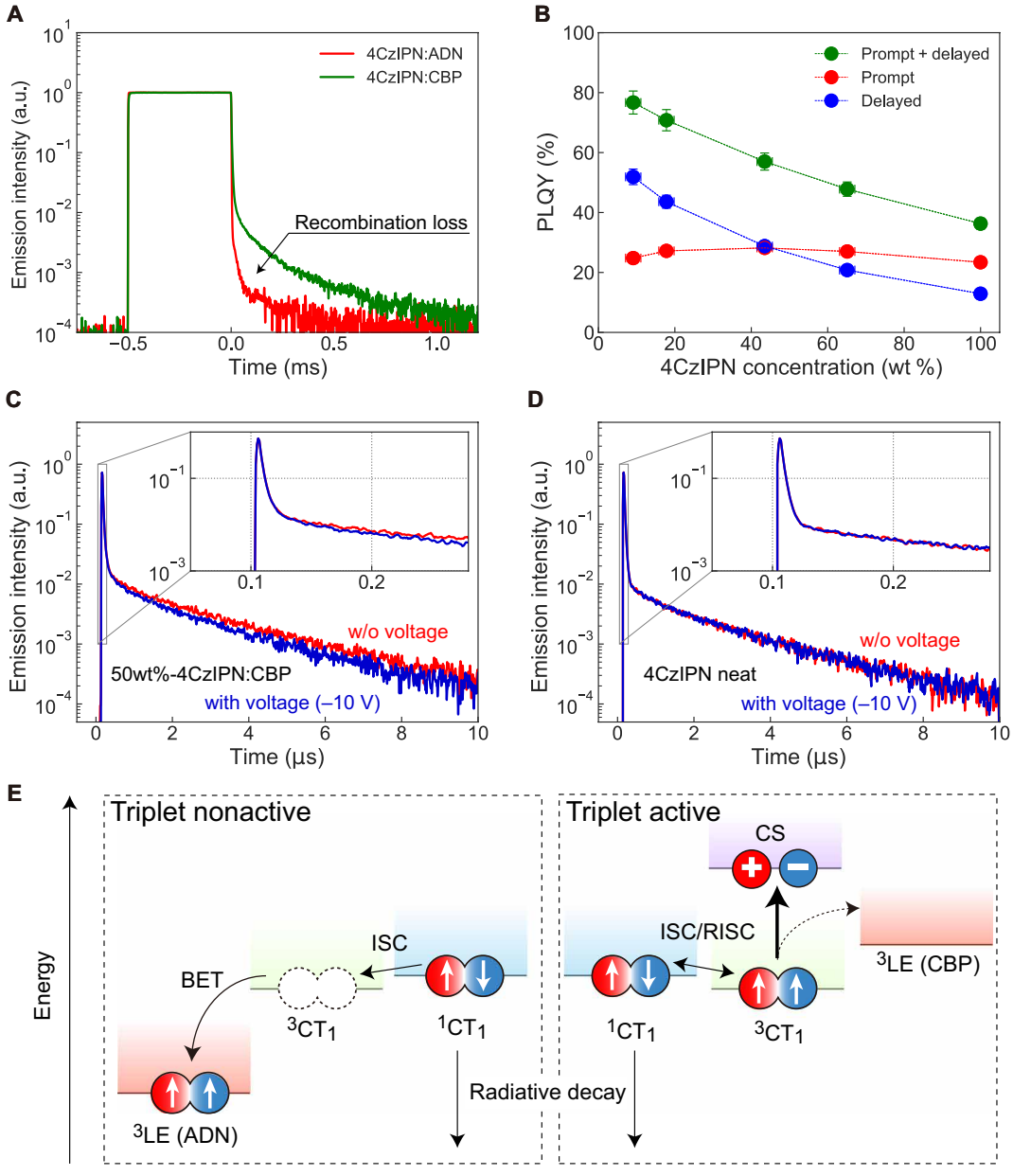

Fig. 3. Photoluminescence characteristics of 4CzIPN in a triplet-activated and deactivated host matrix. (**A**) TRPL profile in 4CzIPN:CBP and 4CzIPN:ADN blend films. The doping concentration of 4CzIPN for each host matrix was fixed at 50 wt %. (**B**) Concentration dependence of PLQY for prompt and delayed components in 4CzIPN:CBP blends. The error bars were estimated by considering experimental variability. (**C** and **D**) Emission decay profiles in NCI devices consisting of 50-wt%-4CzIPN:CBP or 4CzIPN under an electric field. The DC voltage was fixed at −10 V. Delayed fluorescence lifetimes of the 50-wt%-4CzIPN:CBP and the neat 4CzIPN film without voltage are 2.34 and 1.86 μs, respectively. (**E**) Schematic of the role of the excited spin state on the exciton dissociation process. BET, back energy transfer.

4CzIPN NCI device, again indicating a low charge-separation efficiency in the 4CzIPN neat NCI device. This result is supported by the absorbed photon-electron conversion efficiency, namely, a full-wavelength IQE, measurements for the 4CzIPN diodes (fig. S14A). The IQE at the wavelength of 430 nm was elevated from 3 to 26% in the 50-wt%-4CzIPN:CBP diode with an increase in the negative bias, whereas an increase in the low IQE from 2 to 8% was observed for the neat 4CzIPN diode (fig. S14B). Note that the charge separation originated from 4CzIPN is ensured, since the wavelength longer than 420 nm is not absorbed by the hole transport layer of α-NPD (fig. S14C). Moreover, the intensity of the normalized IQE spectra in the 50-wt%-4CzIPN:CBP diode was increased with an increase in the negative bias although that of the neat 4CzIPN diode showed almost no change (fig. S14D). This spectral change means that the acceleration of the triplet exciton dissociation depended on the external electric field. Here, the time constant for the delayed component for the neat 4CzIPN diode is virtually independent of the applied voltage (Fig. 3D) and exciton dissociation from the triplet state is negligible. Instead, the smaller IQE for the neat 4CzIPN diode might be attributable to carrier generation from the hot CT

Table 1. Photophysical properties of 50-wt%-4CzIPN and 4CzTPN in CBP.

Compound	Prompt PLQY (%)	Delayed PLQY (%)	τ_p (ns)	τ_d (μs)	k_r (10^7 s^{-1})	k_{ISC} (10^7 s^{-1})	k_{RISC} (10^5 s^{-1})
CBP:4CzIPN	28.2	28.8	30.3	2.34	0.93	2.37	6.07
CBP:4CzTPN	12.2	3.1	11.6	1.75	1.04	7.55	1.68

state, in which the charge generation is independent of the electric field by the aid of the extremely rapid process with excess energy (*27*).

Returning our attention to Fig. 2C, we observe that the decrease in the PL intensity when the negative voltage pulse was applied is substantially smaller for the 4CzTPN:CBP NCI device than for the 4CzIPN:CBP NCI device despite the similar electrical field. A comparison of the prompt:delay ratio for the doped films reveals that the ratio is 1:1 for the 4CzIPN:CBP film and 4:1 for the 4CzTPN:CBP film (Table 1). Assuming that exciton dissociation from the $^3CT_1$ state is more likely than that from the $^1CT_1$ state, as previously mentioned, the 4CzIPN:CBP NCI device is expected to be more easily quenched because of the large population of the $^3CT_1$ state. The IQE of the 50-wt%-4CzIPN:CBP diode was elevated largely by applying the negative bias, compared to that of the 50-wt%-4CzTPN:CBP diode (fig. S14A). These observations support our hypothesis that the exciton dissociation from the $^3CT_1$ state is critical (Fig. 3E). Here, note that a small IQE value around the visible region has been observed even in the 50-wt%-4CzTPN:CBP diode at 0 V, and it is slightly larger than that of the 4CzIPN:CBP diode. It would be due to the exciton dissociation by the internal electric field induced by the difference of work function on each electrode, and the effective transport of charge carriers in the diode because the highest occupied molecular orbital (HOMO) levels of 4CzTPN and CBP are almost the same.

2) In addition to the initial carrier density in the 4CzIPN:ADN film being reduced, the small amount of charge carriers generated from the 4CzIPN excitons would be consumed as heat by the production of $^3LE_1$ of ADN through the Dexter event. Thus, the LLE intensity became much weaker than that in the 4CzIPN:CBP case. Moreover, the 4CzIPN:ADN NCI device showed no EL response under an applied positive voltage pulse after the excitation light was turned off (fig. S15), whereas a clear response was observed in the 4CzIPN:CBP NCI device. This behavior is well explained using the back-electron transfer channel to describe the energy loss in OPVs (*3*–*7*). In the case of a 4CzIPN:CBP or 4CzTPN:CBP film, the $^3CT_1$ can survive with a long lifetime because of the shut-off of the Dexter energy transfer channel to the host. In addition, a decrease in the LLE intensity was observed in response to the application of an external negative voltage pulse, indicating the redissociation of the excitons of 4CzIPN and the suppression of charge-carrier recombination (fig. S16). Thus, no formation of the host $^3CT_1$ state is responsible for the no energy-loss channel in the triplet's preserved host environment.

DISCUSSION

We investigated the role of the $^3CT_1$ states in organic molecular systems with a small ΔE_{ST} for exciton dissociation events. Our observations highlight that the charge separation following the exciton dissociation from the $^3CT_1$ states rather than the $^1CT_1$ states is inherently critical because the fast decay channels (e.g., the fluorescence decay channel in $^1CT_1$ states) are shut off and the $^3CT_1$ states are spin-forbidden. We expect that our fundamental findings will contribute to the future molecular design of efficient photoelectron conversion via the engineering of the excited spin states. For example, CT excitons exhibiting $k_r << k_{ISC}$ are advantageous for generating long-lived charge carriers and successive exciton dissociation for a high photoelectron conversion efficiency. The molecular structure of 4CzIPN (or 4CzTPN) used in the present study is, unfortunately, unfavorable for charge separation between neighboring molecules because of its four bulky carbazole units, which shield the electron-acceptor unit, and because the $^3CT_1$ state has a short lifetime as a consequence of the nature of the rapid reverse intersystem crossing (*28*). Therefore, for practical applications, the simple D-A–type organic molecular systems that exhibit highly efficient TADF with a long $^3CT_1$ lifetime to provide an efficient carrier separation path, such as *p*-2Cz2BMe ($^3CT_1$ lifetime: millisecond order) (*29*), would become the candidates. Also, we would like to understand the remaining issue for the charge separation processes in D-A intra- and intermolecular CT systems. Other researchers have argued that many intermolecular CT systems show charge separation from their singlet and higher excited states (*4*, *15*, *27*). Systematic studies involving tuning the strength of the CT interaction would clarify the charge separation mechanism conclusively.

MATERIALS AND METHODS

Materials

CBP and T2T were purchased from NARD Institute. α-NPD and Alq_3 were purchased from Nippon Steel Chemical Co. ADN was purchased from Luminescence Technology Corp. 4CzIPN and 4CzTPN were synthesized via previously reported methods (*2*).

Sample preparation

All organic layers were formed by thermal evaporation under high-vacuum conditions ($<10^{-4}$ Pa). Organic films with a thickness of 50 nm were grown on precleaned quartz substrates. All of the devices were fabricated on clean ITO glass substrates and had an effective device area of 4 mm^2. The device structure for the DCM, IQE, and fluorescence lifetime measurements under an electric field was ITO (100 nm)/α-NPD (50 nm)/emissive material layer (EML) (50 nm)/Al (100 nm), with ITO as the anode, α-NPD as the hole transport layer, and Al as the cathode. The device structure for external electric field–modulated PL measurements (NCI-type device) was ITO (100 nm)/T2T (30 nm)/EML (100 nm)/CBP (30 nm)/Al (100 nm), with ITO as the anode, T2T as the hole-blocking layer, CBP as the electron-blocking layer, and Al as the cathode. Each emissive layer consisted of a host matrix (CBP or ADN) and a TADF fluorophore (4CzIPN or 4CzTPN), respectively. After device fabrication, the devices were immediately encapsulated with glass lids and epoxy glue in a dry N_2-filled glove box.

Fundamental PL properties

The PLQY and the time constant for TADF molecules were measured using an absolute PLQY measurement system (C11347-01, Hamamatsu Photonics) and a fluorescence lifetime spectrometer (C11367, Hamamatsu Photonics) with a time-correlated single-photon counting (TCSPC) method, respectively.

TRPL measurement and PL intensity measurement under electric fields

TRPL decay was measured using a photosensor module (H10721-01, Hamamatsu Photonics), an amplifier unit (C11184, Hamamatsu Photonics), and an oscilloscope (WaveRunner 640Zi, Teledyne Lecroy) with a function generator (WaveStation2012, Teledyne Lecroy) as an external electric field source for observing the LLE and external electric field–modulated TRPL profile. A pulsed LED driving circuit was prepared as an excitation source, and a long-pass filter with an optical density of 5 was used for extraction of the sample signal. The power density of the excitation LED was fixed at 20 mW cm^{-2}. All TRPL signals were averaged for 10,000 measurements, smoothed using the moving-average method, and normalized at the intensity immediately before the photoexcitation was turned off.

Fluorescence lifetime measurements under an electric field

The fluorescence lifetime of the samples under an electric field was measured using a photosensor module (H10721-01, Hamamatsu Photonics), an amplifying unit (VT120A, Ortec), a time-to-digital converter (U1050A-002, Agilent), a discriminator (model 584, Ortec), and an excitation light source (LDH-D-C-420, PicoQuant) via the TCSPC method. A DC power supply was used as an external electric field source.

DCM characterization

DCM was conducted using a current-input preamplifier (LI-76, NF Corporation) and a multifunction filter (3611, NF Corp.) with an oscilloscope and a function generator. All DCM curves were measured with a sweep rate of 100 V s^{-1} at room temperature.

IQE measurements

The IQE was calculated as the ratio of the absorbed photons to the observed current. The irradiation power (a tungsten lamp with a monochrometer) was measured using a calibrated photodiode (S1337-1010BQ, Hamamatsu Photonics) covered by a light shield with a 2-mm^2 hole, which was the same area as the active area of the device. The number of absorbed photons was estimated from the absorbance of codeposited films with consideration of the reflection interference and optical length in the device. The photocurrent was measured using a pA Meter DC Voltage Source (4140B, Agilent).

SUPPLEMENTARY MATERIALS

Supplementary material for this article is available at https://science.org/doi/10.1126/sciadv.abj9188

REFERENCES AND NOTES

1. M. A. Baldo, D. F. O'Brien, Y. You, A. Shoustikov, S. Sibley, M. E. Thompson, S. R. Forrest, Highly efficient phosphorescent emission from organic electroluminescent devices. *Nature* **395**, 151–154 (1998).
2. H. Uoyama, K. Goushi, K. Shizu, H. Nomura, C. Adachi, Highly efficient organic light-emitting diodes from delayed fluorescence. *Nature* **492**, 234–238 (2012).
3. T. M. Clarke, J. R. Durrant, Charge photogeneration in organic solar cells. *Chem. Rev.* **110**, 6736–6767 (2010).
4. A. Rao, P. C. Y. Chow, S. Gélinas, C. W. Schlenker, C.-Z. Li, H.-L. Yip, A. K.-Y. Jen, D. S. Ginger, R. H. Friend, The role of spin in the kinetic control of recombination in organic photovoltaics. *Nature* **500**, 435–439 (2013).
5. Y. Hou, X. Zhang, K. Chen, D. Liu, Z. Wang, Q. Liu, J. Zhao, A. Barbon, Charge separation, charge recombination, long-lived charge transfer state formation and intersystem crossing in organic electron donor/acceptor dyads. *J. Mater. Chem. C* **7**, 12048–12074 (2019).
6. S. Gélinas, O. Paré-Labrosse, C.-N. Brosseau, S. Albert-Seifried, C. R. McNeill, K. R. Kirov, I. A. Howard, R. Leonelli, R. H. Friend, C. Silva, The binding energy of charge-transfer excitons localized at polymeric semiconductor heterojunctions. *J. Phys. Chem. C* **115**, 7114–7119 (2011).
7. H. Kraus, M. C. Heiber, S. Väth, J. Kern, C. Deibel, A. Sperlich, V. Dyakonov, Analysis of triplet exciton loss pathways in PTB7:$PC_{71}BM$ bulk heterojunction solar cells. *Sci. Rep.* **6**, 29158 (2016).
8. S. H. Park, A. Roy, S. B. S. Cho, N. Coates, J. S. Moon, D. Moses, M. Leclerc, K. Lee, A. J. Heeger, Bulk heterojunction solar cells with internal quantum efficiency approaching 100%. *Nat. Photonics* **3**, 297–302 (2009).
9. H. Yin, S. Chen, S. H. Cheung, H. W. Li, Y. Xie, S. W. Tsang, X. Zhu, S. K. So, Porphyrin-based thick-film bulk-heterojunction solar cells for indoor light harvesting. *J. Mater. Chem. C* **6**, 9111–9118 (2018).
10. D. Baran, N. Gasparini, A. Wadsworth, C. H. Tan, N. Wehbe, X. Song, Z. Hamid, W. Zhang, M. Neophytou, T. Kirchartz, C. J. Brabec, J. R. Durrant, I. McCulloch, Robust nonfullerene solar cells approaching unity external quantum efficiency enabled by suppression of geminate recombination. *Nat. Commun.* **9**, 2059 (2018).
11. P. C. Y. Chow, S. Gélinas, A. Rao, R. H. Friend, Quantitative bimolecular recombination in organic photovoltaics through triplet exciton formation. *J. Am. Chem. Soc.* **136**, 3424–3429 (2014).
12. J. Benduhn, F. Piersimoni, G. Londi, A. Kirch, J. Widmer, C. Koerner, D. Beljonne, D. Neher, D. Spoltore, K. Vandewal, Impact of triplet excited states on the open-circuit voltage of organic solar cells. *Adv. Energy Mater.* **8**, 1800451 (2018).
13. T. Higashino, T. Yamada, M. Yamamoto, A. Furube, N. V. Tkachenko, T. Miura, Y. Kobori, R. Jono, K. Yamashita, H. Imahori, Remarkable dependence of the final charge separation efficiency on the donor–acceptor interaction in photoinduced electron transfer. *Angew. Chem. Int. Ed.* **55**, 629–633 (2015).
14. M. R. Narayan, J. Singh, Roles of binding energy and diffusion length of singlet and triplet excitons in organic heterojunction solar cells. *Phys. Status Solidi C* **9**, 2386–2389 (2012).
15. A. Classen, C. L. Chochos, L. Lüer, V. G. Gregoriou, J. Wortmann, A. Osvet, K. Forberich, I. McCulloch, T. Heumüller, C. J. Brabec, The role of exciton lifetime for charge generation in organic solar cells at negligible energy-level offsets. *Nat. Energy* **5**, 711–719 (2020).
16. T. Yamanaka, H. Nakanotani, C. Adachi, Slow recombination of spontaneously dissociated organic fluorophore excitons. *Nat. Commun.* **10**, 5748 (2019).
17. Y. Noguchi, W. Brütting, H. Ishii, Spontaneous orientation polarization in organic light-emitting diodes. *Jpn. J. Appl. Phys.* **58**, SF0801 (2019).
18. R. Kabe, C. Adachi, Organic long persistent luminescence. *Nature* **550**, 384–387 (2017).
19. Z. Zhou, C. Qiao, K. Wang, L. Wang, J. Liang, Q. Peng, Z. Wei, H. Dong, C. Zhang, Z. Shuai, Y. Yan, Y. S. Zhao, Experimentally observed reverse intersystem crossing-boosted lasing. *Angew. Chem. Int. Ed.* **59**, 21677–21682 (2020).
20. Y. Zhang, S. R. Forrest, Existence of continuous-wave threshold for organic semiconductor lasers. *Phys. Rev. B* **84**, 241301(R) (2011).
21. S. Egusa, N. Gemma, A. Miura, K. Mizushima, M. Azuma, Carrier injection characteristics of the metal/organic junctions of organic thin film devices. *J. Appl. Phys.* **71**, 2042–2044 (1992).
22. D. L. Dexter, A theory of sensitized luminescence in solids. *J. Chem. Phys.* **21**, 836–850 (1953).
23. L. Jäger, T. D. Schmidt, W. Brütting, Manipulation and control of the interfacial polarization in organic light-emitting diodes by dipolar doping. *AIP Adv.* **6**, 095220 (2016).
24. M. Tanaka, H. Noda, H. Nakanotani, C. Adachi, Molecular orientation of disk-shaped small molecules exhibiting thermally activated delayed fluorescence in host–guest films. *Appl. Phys. Lett.* **116**, 023302 (2020).
25. H. S. Kim, S.-R. Park, M. C. Suh, Concentration quenching behavior of thermally activated delayed fluorescence in a solid film. *J. Phys. Chem. C* **121**, 13986–13997 (2017).
26. J. Lee, N. Aizawa, M. Numata, C. Adachi, T. Yasuda, Versatile molecular functionalization for inhibiting concentration quenching of thermally activated delayed fluorescence. *Adv. Mater.* **29**, 1604856 (2017).
27. A. E. Jailaubekov, A. P. Willard, J. R. Tritsch, W.-L. Chan, N. Sai, R. Gearba, L. G. Kaake, K. J. Williams, K. Leung, P. J. Rossky, X.-Y. Zhu, Hot charge-transfer excitons set the time limit for charge separation at donor/acceptor interfaces in organic photovoltaics. *Nat. Mater.* **12**, 66–73 (2013).
28. H. Noda, X.-K. Chen, H. Nakanotani, T. Hosokai, M. Miyajima, N. Notsuka, Y. Kashima, J.-L. Brédas, C. Adachi, Critical role of intermediate electronic states for spin-flip processes

in charge-transfer-type organic molecules with multiple donors and acceptors. *Nat. Mater.* **18**, 1084–1090 (2019).
29. H. Noda, H. Nakanotani, C. Adachi, Highly efficient thermally activated delayed fluorescence with slow reverse intersystem crossing. *Chem. Lett.* **48**, 126–129 (2019).

Acknowledgments: We acknowledge Y. Ueda for his assistance with preparing the samples and K. Nakamoto for his assistance with fluorescence lifetime measurements. **Funding:** This work was supported in part by the Japan Society for the Promotion of Science (JSPS) KAKENHI grant number JP21H02015 and Core-to-Core program. **Author contributions:** H.N. and T.Y conceived and designed the project. T.Y. prepared the samples and conducted all measurements. T.Y. and H.N. analyzed all the data. C.A. supervised the project. All authors contributed to writing the paper and critically commented on the project. **Competing interests:** The authors declare that they have no competing interests. **Data and materials availability:** All data needed to evaluate the conclusions in the paper are present in the paper and/or the Supplementary Materials.

Submitted 11 June 2021
Accepted 3 January 2022
Published 2 March 2022
10.1126/sciadv.abj9188